Title

Case Study of Parallel Bridges Affected by Liquefaction and Lateral Spreading

Journal
Journal of Geotechnical and Geoenvironmental Engineering, 142(7)

ISSN
1090-0241

Authors
Turner, Benjamin J
Brandenberg, Scott J
Stewart, Jonathan P

Publication Date
2016-07-01

DOI
10.1061/(asce)gt.1943-5606.0001480

Peer reviewed

CASE STUDY OF PARALLEL BRIDGES AFFECTED BY LIQUEFACTION AND LATERAL SPREADING

By Benjamin J. Turner, S.M.ASCE[1], Scott J. Brandenberg, M.ASCE[2], and Jonathan P. Stewart, F.ASCE[3]

ABSTRACT

Two parallel adjacent river-crossing bridges performed differently in response to strong shaking (peak ground acceleration ~0.27g) and liquefaction-induced lateral spreading during the 2010 **M**7.2 El Mayor-Cucapah earthquake. A railroad bridge span collapsed, whereas the adjacent highway bridge survived with one support pier near the river having modest flexural cracking of cover concrete, and a second that settled approximately 50 cm. Cone penetration and geophysical test results are presented along with geotechnical and structural conditions evaluated from design documents. We find an equivalent-static beam-on-nonlinear-Winkler foundation analysis to accurately predict observed responses when liquefaction-compatible inertia demands are represented as spectral displacements that account for resistance from other bridge components. Pier columns for the surviving bridge effectively resisted lateral spreading demands in part because of restraint provided by the superstructure. Collapse of the surviving bridge is predicted when liquefaction-compatible inertial demands are computed for the individual bent in isolation from other components, and are represented by forces instead of displacements. The poor performance

[1] Ph.D. Candidate, Dept. of Civil and Environmental Engineering, Univ. of California at Los Angeles, Los Angeles, CA 90095 (corresponding author). E-mail: bjturner@ucla.edu
[2] Associate Professor and Vice Chair, Dept. of Civil and Environmental Engineering, Univ. of California at Los Angeles, Los Angeles, CA 90095
[3] Professor and Chair, Dept. of Civil and Environmental Engineering, Univ. of California at Los Angeles, Los Angeles, CA 90095

of the settled pier column resulted from bearing capacity failure in a thin liquefiable layer at the shaft tip.

Keywords: *deep foundations; lateral spreading; bridges; inertial demands*

INTRODUCTION

Lateral spreading from the 2010 **M** 7.2 El Mayor-Cucapah earthquake damaged a pair of parallel bridges, separated by only a few meters, in northern Baja California, Mexico. One span of a railroad bridge collapsed, whereas the adjacent highway bridge suffered only minor flexural cracking of columns adjacent to the river and settlement of another bent of columns. These case histories afford an opportunity to assess how well engineering evaluation procedures predict good and poor field performance at a liquefaction site with essentially identical geotechnical conditions and shaking demands. In this study, the response of the bridges to lateral spreading is analyzed using a beam-on-nonlinear-Winkler foundation (BNWF) equivalent-static analysis (ESA) procedure (by Ashford et al., 2011) that is similar to recommended procedures in current U.S. federal and state department of transportation guidelines [e.g., MCEER/ATC-49 (2003) that is referenced by AASHTO (2014); Caltrans 2013]. We also analyze the bent of columns that settled using various assumptions for the end bearing capacity and shaft friction within liquefied layers.

The modeling of bridge response to lateral spreading with an equivalent-static BNWF approach is attractive in practice because it is computationally efficient and requires input parameters that are simpler to develop than those for finite element continuum modeling. However, this simplicity comes at the cost of neglecting some aspects of the true response, mainly related to the transient interactions that occur between laterally spreading soil and structural elements. In other words, all models have limitations, including those considered here, and the practical question is how well a model can capture the most essential aspects of the response that lead to damage. It is this question that is explored using the case studies of the Baja bridges.

Past validation efforts of ESA procedures focused on individual case histories of mostly poor bridge performance (e.g., Berrill et al. 2001; Dobry et al. 2003; Rollins et al. 2005). Fewer studies have validated these procedures against cases of good performance (e.g., Brandenberg et al. 2013), which are of equal value. The present opportunity to validate ESA procedures against case histories of adjacent bridges with distinct performance levels at a single site is unique.

REGIONAL SETTING AND SITE DESCRIPTION

Geologic Setting

The San Felipito Bridges (SFB) cross the Colorado River in the south-central Mexicali Valley in northern Baja California, Mexico, about 60 km south of the city of Mexicali and the border with the U.S. (approximate site coordinates 32.244°N, 115.053°W). The Mexicali Valley and its American counterpart to the north, the Imperial Valley, are "pull-apart basins" or structural depressions that result from divergent fault step-over bends along the boundary between the Pacific and North American plates. The valleys are filled with 10 to 12 km of alluvial sediments from the Colorado River interbedded with marine sediments deposited as the Gulf of California has periodically shifted north (Merriam and Bandy 1965).

Regional tectonics are dominated by right-lateral transform movement along the continental margin connected by a series of roughly east-west trending oblique normal faults that accommodate extension and down dropping. The area is seismically active, with several major recent earthquakes, including an estimated **M** 7.2 event in 1892 (Hough and Elliot 2004). The 2010 El Mayor-Cucapah earthquake began on a short, unnamed normal fault and propagated primarily as strike-slip movement to the southeast along the previously unknown Indiviso fault and northwest along the Pescadores and Borrego faults (GEER 2010; Hauksson et al. 2011).

Bridge and Foundation Configurations

As shown in Fig. 1, the river crossing consists of a highway bridge (HWB) constructed in 1999, and an adjacent railroad bridge (RRB) built in 1962 (EERI 2010). The surrounding area consists mostly of level agricultural fields elevated about 4 to 5 m above the river flood plain, protected from flooding by levees that adjoin the north sides of the approach embankments. The crossing occurs at a broad bend where the river has migrated to the west side of its flood plain, leaving younger, looser sediments on the east bank, which is where the majority of the structural damage occurred that is the focus of this study.

Both bridges consist of precast-prestressed simply supported concrete spans on elastomeric bearings resting atop reinforced concrete bents supported by deep foundations. The bents of the HWB were designed to match the 20-m spacing of the RRB, with ten spans for a total bridge length of 200 m. The primary difference between the two bridges is the size and number of foundations that support each bent, as discussed below. Further details of the bridge configurations and connection details are presented in Turner et al. (2014).

Each bent of the HWB is supported by four 1.2-m-diameter extended-shaft columns that are continuous with drilled shaft foundations (no pile cap) of the same size and reinforcement detail. The foundations in the active river channel extend approximately 17 m below the river surface elevation, as shown in Fig. 2, while the foundations nearest the abutments and beneath the eastern spans where the river flows less frequently are shorter by 3 to 6 m.

Officials from *Secretaría de Comunicaciones y Transportes* (SCT), the Mexican agency responsible for the HWB, provided construction plans, records of geotechnical explorations, structural design documents, and anecdotal reports of the bridge construction (SCT personal communication, 2013). The HWB foundations were built by advancing a temporary steel casing under its own weight or by hydraulic jacking through stiff layers and removing spoils by airlifting. Liquefaction effects such as downdrag and lateral spreading are not mentioned in the design documents, implying that the bridge was not designed for such effects.

Foundation details of the RRB are uncertain, but given the timeframe of construction, the fluvial environment, and the propensity of North American railroad companies to use driven pile foundations (e.g., the post-earthquake repair of the RRB utilized driven steel piles), the pile caps are most likely supported on driven piles as opposed to drilled shafts. Because it is not known whether timber, concrete, or steel piles were used, analyses were performed considering all three materials over a range of sizes and group configurations as explained subsequently. Given the date of construction, it is almost certain that the RRB foundations were not designed to resist the effects of liquefaction and lateral spreading.

Subsurface Conditions

Geotechnical information provided by SCT consists of profiles of soil classification and standard penetration test (SPT) blowcounts for five borings performed in support of the original bridge construction (B-1 through B-5 on Fig. 2) as well as one post-earthquake boring performed adjacent to Bent 6, which settled during the earthquake (PEB-1 in Fig. 2). SCT officials also provided the log of a post-earthquake boring performed by Ferromex, the owner of the RRB, which included grain size distribution laboratory test results.

To better characterize the site conditions, the authors conducted a geotechnical site investigation in October 2013 consisting of cone penetration testing (CPT) with seismic and porewater pressure measurements, test pits for collecting near-surface bulk samples, and spectral analysis of surface waves (SASW) geophysical testing for *in situ* shear wave velocity (V_s) measurement. Four CPT soundings were advanced to depths between 4 and 17 m, and several other attempts were stopped by shallow obstructions. CPT soundings were performed using the NEES@UCLA Hogentogler truck-mounted rig, capable of pushing to a maximum cone tip resistance (q_c) of 30 MPa. Locations of CPT-1 to CPT-4 are shown in Fig. 1 and q_c profiles are shown in Fig. 2.

Considering all the available information, the stratigraphy (Fig. 2) can be summarized as follows: surficial soil consists of a loose, uniformly graded, silty fine sand layer extending to a depth of about 6 m near the river. An unsaturated "crust" is present above the groundwater table, which is about 1.5 to 2 m below the ground surface. In the vicinity of the bridges, the crust soil is highly disturbed from post-earthquake repair efforts, so it is considered fill, although its composition is that of the natural sediments. The fines portion of the soils consist of nonplastic silt (confirmed by Atterberg limits and hydrometer tests) that is expected to behave in a "sand-like" manner. Moving away from the river, the thickness of the loose surface layer decreases and its overburden-normalized penetration resistance increases, suggesting higher relative densities. Below the loose layer, interbedded dense and loose layers continue to the maximum depth of CPT exploration (16.6 m) and a similar interbedded pattern is expected at greater depths. Within the interbedded strata, the dense layers range in thickness from about 1 to 3 m, while the loose layers are generally thinner, ranging from about 0.25 to 1 m thick. The CPT results and index test results shown on the Ferromex boring suggest that the soil at depth has the same general consistency as the near-surface soil, i.e., fine to medium sand with varying amounts of nonplastic to low plasticity fines. Some thin layers of predominantly fine-grained soil are present within the interbedded granular layers.

The stratigraphy that SCT inferred from their borings and SPT measurements conducted prior to bridge construction is somewhat different. Their interpretation was that surficial soils consist of about 6 to 10 m of loose silty sand that gradually increases in relative density with depth. Those materials were interpreted as overlying a very dense layer of silty sand that produced refusal blow counts to the maximum depth of exploration. However, CPT-1 and PEB-1 show that loose layers are interbedded with the dense layers over the depth interval of 10 to 16 m, and the loose layers were found to be susceptible to liquefaction in the analyses performed for this study. Members of the Geotechnical Extreme Events Reconnaissance (GEER) team that performed post-earthquake reconnaissance at the site observed that PEB-1 was advanced by hydraulic jetting (GEER 2010) using river water, which is a non-standard drilling method that may result in erroneous blow count measurements. Given that the near-surface soils at the site include loose non-plastic silts and sands below the water table, borehole caving as SPTs were conducted is possible, which would increase friction along rods, causing erroneously large N-values. This may explain the near-surface refusal blowcounts in PEB-1 (Fig. 2). Similar circumstances may explain the high N-values from pre-event SCT investigations as well (e.g., near-surface refusal in B-4). Accordingly, we do not consider any of the available blow count data to accurately reflect *in situ* conditions, but the logs were valuable to guide our assessment of site stratigraphy.

Two SASW geophysical surveys were conducted at the locations shown in Fig. 1. Four sensors were placed at 2-m and 4-m horizontal spacings to record signals generated by a vertical constant-force shaker performing a sine wave sweep over a frequency range of 5 to 35 Hz. Recordings were also taken with a sledgehammer impacting a steel plate as a high-frequency source. From the SASW and CPT results, time-averaged shear wave velocities were inferred to a depth of approximately 16 m ($V_{S16} \approx$ 160-200 m/s), from which the time-averaged shear wave velocity over the upper 30 m of the site profile (V_{S30}) was estimated to range between approximately 180 and 230 m/s using the extrapolation technique of Boore (2004).

OBSERVED FIELD PERFORMANCE

This section summarizes the findings of reconnaissance teams from GEER and the Earthquake Engineering Research Institute (EERI) that visited the site shortly after the earthquake (GEER 2010; EERI 2010).

Ground Failure

Lateral spreading cracks documented by the GEER team are shown in Fig. 1. The maximum documented lateral spreading surface displacement was 4.6 m towards the east river bank based on summing crack widths at the ground surface along a transect about 60 m north of the bridges. Lateral spreading deformation was observed to be greater on the east bank of the river than the west bank, which is likely because the river currently flows along the western margin of its floodplain so the alluvial sediments on the east bank are younger, looser, and more susceptible to liquefaction. In general, lateral displacements were observed to decrease with increasing distance from the river, as well as in close proximity to the bridges.

At HWB Bent 6, GEER (2010) reported apparent ground settlement relative to the bridge columns of about 30 to 50 cm on the river-side of the columns and 10 to 15 cm on the upslope side of the columns. The Bent 6 columns also settled about 50 cm as evidenced by vertical displacement in the bridge deck. Combined with the apparent relative displacement between the ground and the Bent 6 columns, this indicates that the total ground settlement may have been as much as 0.8–1.0

m. The ground settlement was likely due to a combination of post-liquefaction reconsolidation of the liquefied soil layers and extension/shear strains associated with lateral spreading of the crust. The relative ground-column settlements were estimated based on the assumption that the height of soil adhered to the sides of the columns is representative of the ground level immediately preceding the earthquake. However, there are no means for independently measuring the amount of ground settlement that occurred. Ground settlement likely occurred elsewhere, but no other structural settlement was documented.

Structural Damage

The bents of the RRB closest to the east and west river banks (Bents 5 and 2, respectively) translated toward the river due to lateral spreading, which exceeded the lateral displacement capacity of the elastomeric bearings and led to unseating of the girders for a span on the eastern bank (Fig. 3) and near-collapse of a span on the west bank. The translation was observed to occur with relatively little corresponding column rotation or plastic deformation, indicating that damage was concentrated in the pile foundations. The bridge deck also displaced in the transverse direction relative to the bents, although these displacements were smaller than those in the longitudinal direction.

Damage to the HWB was concentrated in discrete zones and was moderate overall. In contrast to the RRB, the HWB exhibited much better performance; it remained in operation immediately following the earthquake and required repair efforts that were completed with minimal disruption to traffic. The damage documented by the reconnaissance teams is summarized as follows:

(1) Flexural cracking occurred on the inward (river side) of the base of the columns of the bents on both sides of the river, indicating horizontal movement of the foundations towards the center of the river due to lateral spreading (Fig. 3). The bridge deck showed minor cracking above these damaged bents,

(2) Bent 6 settled about 50 cm, which cracked the overlying pavement, and

(3) Shear keys intended to prevent unseating of the girders in the transverse direction were damaged, likely due to transverse inertial demands.

Based on measurements taken during the 2013 site investigation, columns at Bent 5 of the HWB rotated between approximately 0.9° and 1.7° away from the river, i.e., the bottom of the column was displaced towards the river relative to the top of the column. Rotation was smaller for the column nearest the RRB, and largest for the column furthest away. For the remaining HWB bents, pier column rotation consistently decreased with increasing distance from the river. The RRB Bent 5 column, which translated enough to cause unseating of one of the spans it supported, rotated about 0.4° away from the river and about 0.6° to the north; however the rotation was difficult to measure accurately because of the irregular surface of the column. The remaining RRB bents on the east side of the river had no measureable rotation.

ANALYSIS

The San Felipito Bridges (SFB) were analyzed using equivalent static analysis (ESA) procedures recommended by Ashford et al. (2011) so that the analysis results could be compared to observed field performance for validation purposes. The procedures given by Ashford et al. (2011) differ from those recommended in state and federal guidelines documents (e.g., AASHTO 2014; Caltrans 2013) in that Ashford et al. more carefully consider the phasing of effects of liquefaction-induced strength loss and displacements relative to inertial demands. Moreover, Ashford et al. provide a less prescriptive modeling approach. The following were analyzed: (1) HWB Bent 5 with imposed lateral spreading and liquefaction-compatible inertial demands, (2) RRB Bent 5 with imposed lateral spreading and liquefaction-compatible inertial demands, and (3) the axial response of HWB Bent 6.

Analyses were performed using the finite-element modeling platform *OpenSees* (McKenna et al. 2010). In principal, the lateral spreading analysis could be performed with any numerical analysis software that incorporates the BNWF approach and allows the user to impose a ground displacement profile to the free ends of the soil springs to simulate lateral spreading while permitting adequate consideration of important structural details. For example, the California Department of Transportation lateral spreading design guidelines (Caltrans 2013) describe how to perform the analysis using the ENSOFT program *LPILE* (Reese et al. 2005). *OpenSees* was used for this project instead of *LPILE* because (1) it permits more detailed structural modeling (e.g., bearings between piers and girders, rotational stiffness at the top of the column(s), modal analysis, etc.), (2) groups of piles can be modeled explicitly (the authors recognize that ENSOFT also makes *GROUP*, which permits pile group analysis), and (3) it is a free open-source tool that has been widely utilized by the earthquake engineering research community.

Above-ground components of the bridge bents were modeled up to the connections between the columns and the superstructure. An alternative that is often used with the BNWF approach is to decouple the column demands from the foundation demands and impose the estimated column demands on a separate foundation(s)-only model. In cases where ground failure does not occur and foundations solely provide resistance to superstructure loads, a foundation(s)-only model is appropriate. However, explicitly modeling the columns and the connection to the superstructure is preferred for cases involving ground failure because in many cases the lateral spreading demands are resisted in a distributed manner across multiple bridge components as a result of interaction through above-ground structural elements. In particular, abutments and bents founded in nonliquefied soil can provide significant resistance against lateral spread displacements. As a result, characterizing demands at the base of columns *a priori* is often not feasible. Furthermore, our knowledge of the damage to the bridges in this study is based primarily on post-earthquake observations of above-ground structural elements, namely cracking, rotation, and translation of columns. Since this damage was used as the basis for validation of the ESA procedures, it was necessary to include above-ground elements in the model.

Ground Motion Estimation

The SFB site is approximately 14.5 km east of the fault rupture zone. The peak ground acceleration (PGA) values recorded at the three nearest accelerographs are 0.40*g*, 0.15*g*, and 0.29*g* (PEER 2013). Alluvial floodplain deposits at the SFB site are softer than at the locations of these accelerographs, so PGA at the SFB site was estimated using a procedure described by Kwak et al. (2015). In this method, residuals defined as the measured ground motion minus that from a selected ground motion prediction equation (GMPE) are spatially interpolated at the location of interest using a Kriging method. The interpolated residual is then added to the median prediction from the GMPE for the site. Because the GMPE includes a site term, this procedure inherently accounts for differences in site conditions that would be ignored if PGA values were directly interpolated. Using the BSSA 2014 GMPE (Boore et al. 2014), the PGA residual (in natural log units) at the SFB site is about -0.04. The resulting estimated PGA range is 0.26 to 0.27*g*, using estimated V_{S30} values of 180 to 230 m/s, respectively, as shown in Fig. 4. Pseudo-spectral accelerations (PSAs) at the first-mode periods of the bridges were computed in a similar manner to estimate inertial demands.

Liquefaction

A liquefaction susceptibility and triggering analysis following recommendations by Idriss and Boulanger (2008) predicted liquefaction would occur, with the thickness of liquefiable layers decreasing with increasing distance from the river. The results for CPT-1 are shown in Fig. 5. Soil layers with soil behavior type index (I_c) less than 2.6 were assumed susceptible to liquefaction, which is supported by the laboratory tests that showed that the fines fraction of the silty sand consisted of nonplastic silt. The triggering analyses were performed for a PGA range of 0.17 to 0.41g to capture the ground motion uncertainty due to V_{S30} and the within-event aleatory variability [± one within-event standard deviation (ϕ) range considered as shown in Fig. 4] in the estimated shaking intensity. Triggering of liquefaction is predicted in the upper loose sand layer (layer 2 in Table 1) for PGA > ~0.15g; permanent shear deformations producing lateral spreading are also anticipated in that layer. Because triggering occurs at a PGA below the lower bound of the considered range of shaking intensity, the triggering analysis is insensitive to variability in PGA, and only the median estimates of ground motion intensity are used for subsequent analyses.

A tri-linear ground displacement profile approximately corresponding to the maximum observed free-field lateral spreading displacement of 4.6 m was imposed on the free ends of the *p-y* elements for the lateral spreading ESA. The shape of the tri-linear ground displacement profile closely matches the profile of lateral displacement index (LDI) predicted using the method of Zhang et al. (2004), shown in Fig. 5. Larger PGA values between the median and upper-bound of the range considering aleatory uncertainty (0.27 to 0.41 g) do not result in larger predicted LDI, while the lower-bound PGA (0.17 g) results in a predicted LDI that is about 35 percent below the median prediction. The free-field displacements were not reduced to account for “pinning effects” (i.e., reduction of lateral spreading displacement demand at the bridge location relative to the free-field displacement). Ashford et al. (2011) indicate that pinning effects should not be included for interior bents where the out-of-plane width of the spread feature is essentially infinite relative to the bridge transverse dimension, unlike the case where a finite-width approach embankment is resisted by abutment foundations. Free-field lateral spreading displacements estimated using various published procedures varied from 1 to 6 m, which is reasonably consistent with observations. Details are omitted from this paper for brevity, but can be found in Turner et al. (2014).

Excess porewater pressure ratio r_u (ratio of pore pressure to initial vertical effective stress) during earthquake loading was estimated from the liquefaction triggering analysis results using the strain-based approach described by Cetin and Bilge (2012), and the estimated values of r_u (Fig. 5) were used to compute effective stresses for the analyses, including in layers not predicted to fully liquefy.

Geotechnical Properties

Geotechnical parameters were estimated from the CPT data, laboratory index tests, and the shear wave velocity profiles from the 2013 site investigation. Basic soil properties and the correlations used to estimate them are relative density [weighted average of Kulhawy and Mayne (1990) Eqn. 2-21c—30% weight, Zhang et al. (2004)—30%, and Idriss and Boulanger (2008)—40%], unit weight (based on estimated relative density and judgment), and peak friction angle [Bolton (1986) and Robertson (2012)]. The idealized soil profile with selected properties used in lateral spreading analyses is given in Table 1.

Interaction between the soil and foundations was modeled using nonlinear *p-y* springs for lateral loading using the *PySimple1* uniaxial material model in *OpenSees*. For the RRB, *t-z* and *Q*-

z springs were used to model axial side and base resistance of the piles using the *TzSimple1* and *QzSimple1* materials, respectively. For the HWB, axial resistance did not affect the response to lateral spreading since axial-interaction group effects were not a factor for the single row of extended-shaft columns.

For the *p*-*y* springs, initial stiffness, ultimate resistance (p_{ult}), and relative displacement between the pile and soil when 50 percent of p_{ult} is mobilized (y_{50}) were computed from the values of relative density and peak friction angle presented in Table 1 using the API (1993) sand formulation. The *t*-*z* springs are based on the backbone curve defined for sand by Mosher (1984) with an ultimate resistance based on the effective stress at the spring depth and assumptions of at-rest lateral earth pressure (K_0) conditions, computed as (Jaky 1944):

$$K_0 = 1 - \sin\phi' \tag{1}$$

where ϕ' is the peak friction angle given in Table 1, and interface friction angle equal to the peak friction angle following the recommendations of Brown et al. (2010). Although the lateral earth pressure may exceed the at-rest condition for the driven piles that are assumed to support the RRB, simulations using K_0 indicated the foundations have adequate side resistance to resist overturning, which matches the post-earthquake observations well. Any additional axial resistance arising from higher interface normal stress would not change this outcome. *Q*-*z* springs following the functional form of Vijayvergiya (1977) were created based on a unit base resistance $\left(q_b\right)$ estimated from the CPT data using the following equation (Salgado 2006):

$$q_b = c_b q_{cb} \tag{2}$$

where q_{cb} is the cone tip resistance at the pile base level, and c_b is a constant that quantifies the ratio of base resistance to cone tip resistance based on soil type and pile material. Unit base resistance was computed considering a range of c_b values between 0.25 and 0.5 based on the recommended values in Salgado (2006) and a range of q_{cb} values between 1,500 and 15,000 kPa based on cone tip resistance in the alternating loose/dense layers. These ranges reflect the uncertainty in the RRB pile length, material, and end condition (i.e., full displacement versus open pipe piles). The analysis results were found to be insensitive to the chosen value of base resistance since the majority of the axial resistance of the piles comes from side resistance.

The *t*-*z* and *Q*-*z* springs are based on the assumption that 50% of the spring's ultimate resistance is mobilized at relative displacements (z_{50}) of 1.5 mm and 1.25% of the foundation diameter, respectively. These z_{50} values imply that the full resistance of the *t*-*z* and *Q*-*z* springs will be mobilized at relative displacements of about 1.5 cm and 10% of the foundation diameter, respectively.

The influence of liquefaction on *p*-*y* behavior was accounted for by multiplying the computed p_{ult} by the *p*-multiplier values (m_p) presented in Table 1, which range between 0.14 and 0.28 for the liquefied layers following the recommendations of Brandenberg (2005). The *p*-multipliers were also applied to the *t*-*z* springs per the recommendations of Ashford et al. (2011). To account for the buildup of excess porewater pressure during shaking in nonliquefied layers, *p*-multipliers (m_p) were linearly interpolated between values corresponding to full liquefaction (i.e., $m_{p,liq}$) and the estimated r_u using the following equation (after Dobry et al. [1995]):

$$m_p = 1 - r_u \left(1 - m_{p,liq}\right) \tag{3}$$

The *p*-multipliers recommended by Brown et al. (2010) to account for the "shadowing" effect experienced by trailing rows of piles located behind the lead row (i.e., the traditional use for *p*-multipliers) were also applied in non-liquefied layers. The *p*-*y* curves for the nonliquefied crust layer were formulated to have a resultant force equivalent to a Rankine passive earth pressure wedge acting over the transverse width of the pile group/cap between the ground surface and the groundwater level as described in Turner et al. (2014).

Structural Modeling

Structural properties of the HWB elements are based on the dimensions and material properties shown on the construction plans provided by SCT (Table 2). Construction plans for the RRB were not available, so measurements were taken of the above-ground components during the 2013 investigation. The RRB foundations could not be visually inspected, and foundation type is unknown. However, considering that the bridge was constructed in 1962 by a railroad authority, it is most likely supported on groups of driven piles. Since the foundation type is unknown, a list of pile group configurations and material properties spanning the likely range of foundations installed for the RRB was compiled (Table 3), and all of these cases were analyzed.

The extended-shaft columns of the HWB and the piles and columns of the RRB were modeled as nonlinear beam-column elements idealized as bilinear with pre- and post-yield stiffness and yield moment based on moment-curvature analyses that modeled concrete cracking and steel rebar yielding and strain-hardening. For the timber and steel piles considered for the RRB, a yield stress of 11 MPa and 414 MPa (i.e., Grade 60 steel), respectively, were used in the moment-curvature analysis. Pile caps and bent caps were modeled as elastic beam-column elements. Each structural element was discretized into 0.1-m-long segments, and five integration points were used for interpolating the element response. Translational and rotational restraint provided by elastomeric bearings and shear keys (HWB only) were modeled at the connection between the columns and superstructure as shown in Fig. 6(c). Calculation of the tributary stiffness values assigned to the rotational and translational springs, which in some cases involve multiple components acting in parallel, are not shown here due to space constraints but are explained in detail in Turner et al. (2014). The finite element analyses in *OpenSees* were performed using penalty constraints to enforce boundary conditions, using the norm of the displacement increment (*NormDispIncr* command) to test for convergence with a tolerance of 10^{-8} m, and using a Newton-Raphson solution algorithm. A "*P*-delta" transformation was utilized to capture moments induced by offset axial loads.

Since the HWB bents consist of four identical extended-shaft columns with approximately equal tributary loads, the analysis was performed for a single shaft, and the results are assumed to represent the behavior of all four shafts at the bent. The RRB bents consist of a single column supported on a foundation consisting of a pile cap assumed to connect multiple rows of piles. To accurately capture the foundation group-interaction effect (i.e., the overturning resistance provided by the axial load in each row of piles times its eccentricity from the pile cap centroid), the system was explicitly modeled with multiple rows of piles. Each transverse row of piles for the RRB is represented by a single pile with a flexural rigidity (*EI*) equal to the *EI* of a single pile times the number of piles in the transverse row. The number of piles per row is unknown and is investigated through sensitivity analysis as discussed further below.

Superstructure Inertial Demands

Some fraction of the peak inertial demands are expected to occur simultaneously with kinematic demands imposed by lateral spreading (e.g., Brandenberg et al. 2005). The approach suggested by Ashford et al. (2011) differs from the Caltrans (2013) guidelines regarding modeling of liquefaction-compatible inertial demands, and some discussion is warranted here. Ashford et al. (2011) distinguish pier columns that are not restrained by the superstructure from those that are restrained. Inertial demands for unrestrained pier columns can be represented either as spectral displacements or as inertial forces (Fig. 6). Inertial demands for restrained pier columns are represented as spectral displacements using either a global analysis, or a local analysis with appropriate displacement demands. Inertial demands are estimated first for the non-liquefied condition, and are subsequently reduced to account for (1) the influence of liquefaction on ground surface motion, and (2) phasing between kinematic and inertial demands, which tend to peak at different times. By contrast, the Caltrans (2013) guidelines do not distinguish restrained from unrestrained pier columns, and specify that the liquefaction-compatible inertial demands must be modeled as forces imposed on a foundation(s)-only model rather than as displacements at the superstructure level. In the Caltrans approach, shown in Fig. 6(a), superstructure acceleration at the first mode natural period is determined from a design response spectrum and subsequently reduced by 50% to approximately account for liquefaction and phasing effects. The reduced acceleration demand is then multiplied by the appropriate tributary mass to obtain the liquefaction-compatible inertial demand imposed through the column at the foundation level, with the inertial demand limited by the column plastic moment capacity if flexural yielding is expected.

The force-based approach is problematic for cases where the pier columns are restrained by the superstructure because the pier columns may help resist lateral spreading demands, thereby reducing demands on the foundations while simultaneously increasing demands on the pier columns. Restrained bridge piers have been damaged in past earthquakes when the foundation displacement exceeds the superstructure displacement due to lateral spreading demands (e.g., the Landing Road Bridge; Berrill et al. 2001). The displacement-based approach is more realistic in this regard because (1) the loads mobilized in above-ground components are an outcome of the analysis rather than a prescribed boundary condition, and (2) the spectral displacement accounts for the influence of other bridge components on the global dynamic response. For these reasons, we utilize the displacement-based procedure in this paper, and subsequently demonstrate that the force-based procedure results in an overestimate of foundation demands.

Inertial demands were estimated based on the first-mode natural period of the bridge oscillating in the longitudinal direction obtained from a modal analysis of the system depicted in Fig. 6(c) performed using the *eigen* command in *OpenSees*. The spring shown in Fig. 6(c) at the superstructure level represents the tributary stiffness of the abutment, taken as the cumulative stiffness of the abutment-seat bearings divided by the number of bents and the number of columns per bent (since for the HWB, a single extended-shaft column is analyzed instead of the whole bent). Note that no evidence of pounding was observed at the abutment-deck connections, e.g. complete closure of the gap between the abutment and deck, which would have partially mobilized passive soil resistance against the abutment wall in addition to the elastomeric bearing stiffness. This assumption permitted analysis of the global response of the bridge with a local modal analysis of a single bent. The single-bent models also include translational and rotational springs to capture the column-to-superstructure connection stiffness.

The resulting first-mode periods were used to estimate spectral displacement demands (Fig. 4), which were multiplied by the liquefaction and phasing factors from Ashford et al. (2011). In the equivalent static analyses, this liquefaction-compatible spectral displacement demand was applied at the top of the pier column bearing elements in combination with kinematic lateral spreading demands as shown in Fig. 7. Analyses were performed in which the superstructure displacement demands were applied in (1) the same and (2) the opposite direction of lateral spreading displacement, which produced different results in terms of maximum foundation displacement and flexural demands, respectively.

RESULTS

Performance of Foundation-Column-Superstructure System in Response to Lateral Spreading

Computed responses of the HWB is summarized in Fig. 7. The peak mobilized bending moment near the ground surface was 1,130 kN·m, which lies between the cracking moment of 620 kN·m and the yield moment of 2,000 kN·m. This is consistent with field observations that cracks formed on the river-side of the columns, but that a plastic hinge did not form and residual rotation was minimal. A slightly smaller negative moment was predicted at the interface between the upper liquefied sand layer and the underlying dense sand, -910 kN·m. Whether cracks exist in the extended-shaft columns below the ground level is unknown because the columns were not inspected below grade.

The HWB foundations have sufficient embedment into the dense bearing layer and sufficient stiffness and strength to resist large ground deformation, mobilizing the full passive pressure of the crust layer. Therefore, structural displacements were small and the relative horizontal displacement between the foundations and the laterally spreading crust predicted in the analysis was nearly equal to the free-field ground displacement. The mobilization of full passive pressure is predicted to occur at imposed free-field lateral spreading displacement demands greater than about 0.6 m. Lateral spreading displacements in excess of this amount do not contribute additional structural demands, therefore the results plotted in Fig. 7 are nearly identical to the predicted results for any imposed lateral spreading demand greater than about 0.6 m.

Using the Caltrans (2013) force-based procedure for quantifying inertial demands, the HWB columns were predicted to yield at their base as shown in Fig. 8. When combined with lateral spreading demands, collapse of the HWB was predicted, which is inconsistent with observations. This erroneous prediction is an outcome of prescribing inertial demands as forces rather than displacements and failing to model translational and rotational restraint at the top of the columns, which allows loads to be distributed to other components through the deck. Note that column demands presented in Fig. 7 arise from the combination of inertial loading and lateral spreading; such insight is not provided with a foundation(s)-only model in which column demands are prescribed as boundary conditions in the force-based approach. Fig. 8 demonstrates that collapse is predicted using the force-based method whether the inertial demands are imposed in the same direction as the lateral spreading or in opposite directions, whereas the results utilizing the displacement-based approach are relatively insensitive to the direction of inertial demands and match the observed behavior well in both cases.

Response of the RRB to combined inertial and lateral spreading demands are summarized in Fig. 9. Baseline analyses apply for the assumed condition of multiple rows of piles, as shown in Fig. 9. These analyses show that in contrast to the HWB, the RRB foundations were not capable of resisting the passive pressure of the crust acting against the pile cap. The resulting foundation displacements are large, hence relative displacement between the structure and the laterally spreading crust is low (as seen in Fig. 9), and the full passive pressure mechanism was not mobilized. Moreover, this analysis correctly predicts that Bent 5 of the RRB would translate enough to cause unseating collapse of the span between Bents 5 and 6 under imposed lateral spreading demands greater than or equal to about 1 m for all of the pile material and group configurations considered (recall that actual lateral spread displacements in the free-field at the location of Bent 5 were approximately 4.6 m). Translations at the top of the bent greater than 0.85 m relative to the superstructure are required to cause unseating. After the collapse mechanism has formed, results from the equivalent static analysis for further increases in lateral spreading displacement demand are no longer meaningful. Accordingly, the analyses are terminated at a lateral spreading displacement demand of 1 m rather than extending to the full free-field lateral spreading of 4.6 m.

The large horizontal displacement demand imposed on the RRB foundations by laterally spreading soil is predicted to cause formation of plastic hinges in the piles at the pile cap connections and at the interface between the dense sand layer and the overlying liquefied layer in the simulations. The analysis predicts relatively small column rotations (about 1° or less) even at large horizontal displacements, which is consistent with the observed performance. The lack of rotation is attributed to the rotational restraint provided by the overturning resistance of the pile group and the weight of the superstructure. The lack of rotation associated with such significant translation was a feature of the observed response that was initially perplexing but is explained by the simulations.

Additional simulations were performed using only one row of piles or two closely-spaced rows of piles. Under these assumptions, the pile groups lack significant overturning resistance through group interaction in the bridge longitudinal direction. The result is predictions of large column rotations, even with the restraint provided to the top of the column from the superstructure, which is contrary to observations.

The collective results for the RRB demonstrate that (1) the structure is predicted to collapse over a wide range of foundation types and (2) the observed behavior is best explained by a group of piles with multiple rows that have a large overturning resistance through group interaction but relatively low individual stiffness and strength such that the piles are displaced horizontally and plastic hinges form. Turner et al. (2014) present further details of the parametric studies for various foundation configurations.

Axial Settlement of Highway Bridge Bent 6

The settlement of Bent 6 of the HWB is attributed to a bearing capacity failure associated with decreased side and base resistance in layers that experienced excess porewater pressure generation during the earthquake. Documents provided by SCT indicate that each shaft was designed to carry an allowable axial load of about 2,100 kN. Based on the construction plans, the axial dead load supported by each shaft is about 1,050 kN, consistent with a static factor of safety against axial geotechnical failure of 2.0. However, this does not consider the self-weight of the column, and is significantly less than our estimate of the axial resistance in the absence of liquefaction.

Two cases are considered to evaluate whether a geotechnical failure could have resulted in the observed settlement. The first case essentially represents the original foundation design assumption that the sand is continuously dense below a depth of about 10 m. For this case, the dense soil at the depth of the foundation tips did not liquefy during the earthquake, and all of the layers above the foundation tip contributed drag loads in the same direction as the applied axial load (downward) based on static strengths corresponding to the end of reconsolidation. Although it is unlikely that all the overlying layers would contribute drag loads, this scenario represents the maximum possible axial load at the foundation tip depth. This scenario is presented simply to demonstrate that if the shaft bases were indeed founded in dense soil that did not undergo strength loss, the available base resistance alone (about 13,000 kN) is sufficient to carry the maximum applied axial load (about 3,500 kN) by a factor of almost three, even with the conservative assumption that all layers apply dragload. Hence, plunging failure would not have occurred.

In the second considered case, a loose layer is present at the foundation tips, as indicated by the post-earthquake boring performed by SCT and our CPT sounding at the adjacent Bent 5. We assumed that this loose layer would liquefy based on the results of liquefaction triggering analyses performed using data from CPT-1 for a similar depth range. Axial side and base resistance were computed for the appropriate liquefied/non-liquefied conditions by explicitly considering r_u in the computation of effective stresses. Since the layer at the shaft base was assumed to liquefy, we assumed that all overlying layers contributed drag loads.

When liquefied soil is present at the tip, the reduced base resistance (35 to 185 kN for the range of residual undrained strengths considered) in combination with the shaft friction resistance (950 to 1,300 kN range considered) is smaller than the applied load at the ground surface (1,900 kN, including the column self-weight); drag loads from post-liquefaction reconsolidation would further lower the safety margin. Accordingly, a bearing capacity failure is predicted. Under such conditions, the foundation would "plunge" through the weak material underlying the base until it reaches a denser layer that provides sufficient base resistance to carry the axial load. The magnitude of settlement (about 0.5 m) and the thickness of the potentially liquefiable layers in the vicinity of the shaft tip (about 0.25 to 0.5 m) are roughly equivalent, so this failure mechanism can explain the observed settlement.

Given that the presence of loose layer(s) in the vicinity of the foundation tip depth can explain the observed behavior well, we believe that significant strength loss of these layers occurred during the earthquake, causing a plunging failure. Even if the soil at the shaft tip did not completely liquefy (i.e., r_u did not reach 100%), generation of significant excess porewater pressure could still reduce the bearing capacity of the soil, which would cause settlement if the total resistance drops below the applied load. This failure mechanism is consistent with similar observations by Knappett and Madabhushi (2008) during centrifuge tests of model pile groups in liquefied sand. Had the Bent 6 foundations been a different length such that their tips were not coincident with a loose layer, the failure likely would not have occurred. Ironically, a shorter foundation length may have satisfied this criterion, provided that the shaft tip was founded in a nonliquefied layer thick enough to prevent punching failure.

CONCLUSIONS

The equivalent-static analysis method as described by Ashford et al. (2011) and implemented herein captured both the good performance of the highway bridge and poor performance of the railroad bridge in response to lateral spreading. The differences in performance are explained by relative difference in foundation stiffness and flexural capacity compared to the magnitude of fully-mobilized passive pressure of the crust.

This case study demonstrates several lessons with broad applicability:

- The equivalent-static BNWF approach is a valuable tool for estimating foundation shear and moment demands for structural design, as well as for predicting displacements and rotations for performance evaluation. However, proper implementation of the method requires correctly modeling both the soil and the structural elements that resist lateral spreading demands, which likely includes above-ground bridge components. This requires geotechnical and structural expertise and can best be achieved using software that allows explicit modeling of structural components and connections, such as *OpenSees*.

- Large ground displacements occurred at the site, and the RRB was not stable against the passive pressure of the laterally spreading non-liquefied crust layer. Since there is considerable uncertainty in estimating lateral spreading displacements, if significant lateral spreading is expected at a site (i.e., several meters or more), it is reasonable to assume that enough displacement will occur to fully mobilize passive pressure of a crust layer. Proposed foundation designs should therefore exhibit tolerable rotation and displacement (i.e., be stable) in response to the fully-mobilized demand. In most cases, a stable design will prevent yielding of the foundations and columns; where column or foundation yielding is permitted, significant ductility capacity is required.
- Modeling superstructure inertial demands as the base shear and overturning moment of a laterally-unrestrained SDOF bent model can result in erroneous overestimates of foundation demands. Inertial demands are better represented as spectral displacements at the superstructure level. These spectral displacement demands should be generated from a modal analysis which explicitly considers bridge restraint from all bridge components.
- Axial failure of Bent 6 of the HWB could potentially have been prevented by using a measure of penetration resistance with greater resolution than typical SPT sampling intervals, which would have identified the loose layer near the foundation tip. More suitable exploratory techniques in heterogeneous alluvial environments include CPT or continuous SPT sampling.
- Analysis of axial behavior of deep foundations during seismic loading should explicitly consider generation of excess porewater pressure for computation of effective stress even if full liquefaction is not predicted.

ACKNOWLEDGEMENTS

Financial support for this study was provided by the Pacific Earthquake Engineering Research Center (PEER) Lifelines Program, which receives funding from Caltrans and the Pacific Gas & Electric Company. We would like to acknowledge Tom Shantz from Caltrans, Enrique Hernandez Quinto and Ramón Pérez Alcalá from SCT, Raúl Flores Berrones from IMTA, Alberto Salamanca and Bob Nigbor from UCLA, Chris Krage from UC Davis, and Bill and Kathy Brandenberg for their assistance during the project. The contents of this paper do not necessarily reflect the opinions of the sponsors involved.

REFERENCES

AASHTO (2014). *Guide Specifications for LRFD Seismic Bridge Design, 2nd ed.*, American Association of State Highway Transportation Officials, Washington, D.C.

API (1993). *Recommended Practice for Planning, Design, and Constructing Fixed Offshore Platforms, API RP 2A-WSD*, 20th ed., American Petroleum Institute, API Publishing Services, Washington D.C.

Ashford S.A., Boulanger R.W., and Brandenberg S.J. (2011). Recommended design practice for pile foundations in laterally spreading ground, *PEER Report 2011/04*, Pacific Earthquake Engineering Research Center, University of California, Berkeley, CA, 43 pgs.

Berrill, J.B., Christensen, S.A., Keenan, R.P., Okada, W., and Pettinga, J.R. (2001). "Case study of lateral spreading forces on a piled foundation." *Geotechnique*, 51(6), 501–517.

Bolton M.D. (1986). "The strength and dilitancy of sands." *Géotechnique*, 36(1), 65–78.

Boore D.M. (2004). "Estimating V_s(30) (or NEHRP site class) from shallow velocity models (depths < 30 m)." *Bulletin of the Seismological Soc. of America*, 94(2), 591-597.

Boore D.M., Stewart J.P., Seyhan E., and Atkinson G.M. (2014). "NGA-West 2 equations for predicting PGA, PGV, and 5%-damped PSA for shallow crustal earthquakes." *Earthquake Spectra*, 30(3), 1057-1085.

Brandenberg S.J. (2005). *Behavior of Pile Foundations in Liquefied and Laterally Spreading Ground*, Ph.D. thesis, Department of Civil and Environmental Engineering, University of California, Davis, CA.

Brandenberg S.J., Zhao M., and Kashighandi P. (2013). "Analysis of three bridges that exhibited various performance levels in liquefied and laterally spreading ground." *J. Geotech. Geoenviron. Eng.*, 10.1061/(ASCE)GT.1943-5606.0000832, 1035–1048.

Brown D., Turner J.P., Castelli R. (2010). "Drilled shafts: construction procedures and LRFD design methods." *FHWA/NHI Publication 10-016*, Reference Manual and Participants Guide for National Highway Inst. Course 132014, 972 pgs.

Caltrans (2013). *Guidelines on Foundation Loading and Deformation due to Liquefaction Induced Lateral Spreading*, California Department of Transportation, Sacramento, CA, available: http://www.dot.ca.gov/research/structures/peer_lifeline_program/

Cetin K.O., and Bilge H.T. (2012). "Cyclic large strain and induced pore pressure models for saturated clean sands." *J. Geotech. Geoenviron. Eng.*, 10.1061/(ASCE)GT.1943-5606.0000631, 309-323.

Dobry R., Taboada V., and Liu L. (1995). "Centrifuge modeling of liquefaction effects during earthquakes." *Proc., 1st International Conference on Earthquake Geotechnical Engineering*, K. Ishihara, ed., A.A. Balkema, Rotterdam, 3: 1291–1324.

Dobry, R., Abdoun, T., O’Rourke, T.D., and Goh, S.H. (2003). “Single piles in lateral spreads: Field bending moment evaluation.” *J. Geotech. Geoenviron. Eng.*, 10.1061/(ASCE)1090-0241(2003)129:10(879), 879–889.

EERI (2010). “The El Mayor Cucapah, Baja California earthquake, April 4, 2010.” Earthquake Engineering Research Institute, J. Meneses, ed., *EERI Reconnaissance Report 2010-02*.

GEER (2010). “Preliminary report on seismological and geotechnical engineering aspects of the April 4 2010 Mw 7.2 El Mayor-Cucapah (Mexico) earthquake.” Geotechnical Extreme Event Reconnaissance, J.P. Stewart and S.J. Brandenberg, eds., *Report No. GEER-023.*

Hauksson E., Stock J., Hutton K., Yang W., Vidal-Villegas J., and Kanamori H. (2011). “The 2010 M 7.2 El Mayor-Cucapah earthquake sequence, Baja California, Mexico and Southernmost California, USA: active seismotectonics along the Mexican Pacific Margin.” J. *Pure Appl. Geophys.*, 168(8/9), 1255–1277.

Hough S.E., and Elliot A. (2004). “Revisiting the 23 February 1892 Laguna Salada earthquake.” *Bull. Seismol. Soc. Am.*, 94(4): 1571–1578.

Idriss I.M., and Boulanger R.W. (2008*). Soil Liquefaction during Earthquakes*, Monograph MNO-12, Earthquake Engineering Research Institute, Oakland, CA.

Jaky J. (1948). “Pressure in silos.” *Proc., 2nd International Conference on Soil Mechanics and Foundation Engineering*, Balkema, Rotterdam, 1: 103–107.

Knappett, J. and Madabhushi, S. (2008). “Liquefaction-induced settlement of pile groups in liquefiable and laterally spreading soils.” *J. Geotech. Geoenviron. Eng.*, 10.1061/(ASCE)1090-0241(2008)134:11(1609), 1609–1618.

Kulhawy F.H., and Mayne P.W. (1990). *Manual on Estimating Soil Properties*, *Report EL-6800*, Electric Power Research Institute, Palo Alto, CA.

Kwak, D.Y., Stewart, J.P., Brandenberg, S.J., and Mikami, A. (2015) “Characterization of seismic levee fragility using field performance data.” *Earthquake Spectra*, doi: http://dx.doi.org/10.1193/030414EQS035M.

MCEER/ATC-49 (2003). “Recommended LRFD guidelines for the seismic design of highway bridges.” Multidisciplinary Center for Earthquake Engineering Research, *Report No. MCEER-03-SP03*.

McKenna F.T., Scott, M.H., and Fenves, G.L. (2010). “Nonlinear Finite-Element Analysis Software Architecture Using Object Composition.” *Journal of Computing in Civil Engineering*, 10.1061/(ASCE)CP.1943-5487.0000002, 95-107.

Merriam R., and Bandy O.L. (1965). “Source of upper Cenozoic sediments in Colorado Delta region.” *J. Sediment. Res.*, 35(4): 911–916.

Mosher R.L. (1984). *Load Transfer Criteria for Numerical Analysis of Axial Loaded Piles in Sand*, U.S. Army Engineering and Waterways Experimental Station, Automatic Data Processing Center, Vicksburg, Miss.

Pacific Earthquake Engineering Research (PEER) Center (2013). *NGA-West2 database flatfile*. Available: http://peer.berkeley.edu/ngawest2/databases/. Last accessed 20 November 2013.

Reese L.C., Wang S.T., Isenhower W.M., Arrelaga J.A., and Hendrix J.A. (2005). *LPILE plus version 5.0*. Ensoft, Inc., Austin, TX.

Robertson P.K. (2012). “Interpretation of in-situ tests—some insights.” *Proc., 4th International Conference on Geotechnical and Geophysical Site Characterization (ISC-4),* R.Q. Coutinho and P.W. Mayne, eds., Pernambuco, Brazil, 22 pgs.

Rollins, K. M., Gerber, T. M., Lane, J. D., and Ashford, S. (2005). “Lateral resistance of a full-scale pile group in liquefied sand.” *J. Geotech. Geoenviron. Eng*., 10.1061/(ASCE)1090-0241(2005)131:1(115), 115–125.

Salgado R. (2006). *The Engineering of Foundations,* McGraw-Hill, New York. 882 pgs.

Turner B., Brandenberg S.J., and Stewart J.P. (2014). “Evaluation of collapse and non-collapse of parallel bridges affected by liquefaction and lateral spreading.” *PEER Report 2014/10,* Pacific Earthquake Engineering Research Center, University of California, Berkeley, CA, 122 pgs.

Vijayvergiya V.N. (1977). “Load-movement characteristics of piles.” *Proc., Ports '77: 4th Annual Symposium of the Waterway, Port, Coastal, and Ocean Division*, Long Beach, CA, pp. 269–284.

Zhang G., Robertson P.K., Brachman R.W.I. (2004). “Estimating liquefaction-induced lateral displacement using the standard penetration test or cone penetration test.” *J. Geotech. Geoenviron. Eng.*, 10.1061/(ASCE)1090-0241(2004)130:8(861),861-871.

Table 1: Estimated soil properties for Bent 5 lateral spreading analyses.

Layer	**Description**	**Depth range (m)**	**Unit wt. (kN/m^3)**	D_r **(%)**	**Peak friction angle**	N_{60}	r_u **(%)**	$m_{p,liq}$	m_p
1	unsaturated silty sand crust	0–1.5	17	55	35°	10	N/A	N/A	N/A
2	loose sand	1.5–6.5	18	42	35°	8	100	0.14	0.14
3	dense sand	6.5–8.4	18	77	40°	27	40	0.47	0.93
4	medium-dense sand	8.4–11.2	18	54	37°	20	100	0.28	0.28
5	very dense sand	>11.2	19	82	41°	44	5	0.70	0.98

Table 2: Structural Properties for Lateral Spreading Analysis, Highway Bridge

Element	**Dimensions**	**Flexural Rigidity**[a] **(*EI*) (MN•m^2)**	**Yield moment** M_{yield} **(kN•m)**
Highway Bridge Extended-Shaft Columns	1.2-m diam., 3-m center-to-center spacing (2.5 diam.) 9.2-m column height 17.5-m foundation length	622	2,000
RR-Bridge Oblong Pier Wall Column	8.1-m height 3.0-m x 1.1-m plan dims.	1,530	5,080

[a] Represents cracked sections properties for reinforced concrete sections.

Table 3: Structural Properties for Lateral Spreading Analysis, Railroad Bridge

Element	**Dimensions**		**Flexural Rigidity**[a] **(*EI*) (MN•m^2)**	**Yield moment** M_{yield} **(kN•m)**
RR-Bridge Pile Foundations[b,c] (Case #)	(1)	4x5 group of timber piles, *D* = 30cm, *L* = 10m, *CCS* = 4/4.5	2.8	30
	(2)	4x5 group of RC piles, *D* = 30cm, *L* = 10m, *CCS* = 4/4.5	11	58
	(3)	4x5 group of RC piles, *D* = 30cm, *L* = 15m, *CCS* = 4/4.5	11	58
	(4)	2x5 group of RC piles, *D* = 30cm, *L* = 10m, *CCS* = 12/4.5	11	58
	(5)	4x5 group of steel piles, *D* = 30cm, *L* = 10m, *WT* = 1 cm, *CCS* = 4/4.5	19	265
	(6)	4x5 group of steel piles, *D* = 30cm, *L* = 10m, *WT* = 2cm, *CCS* = 4/3	35	480

[a] Represents cracked sections properties for reinforced concrete sections.
[b] Range of properties considered in analyses due to uncertainty with regards to actual foundation properties
[c] Abbreviations used in table: *D* = diameter, *L* = length, RC = reinforced concrete, *WT* = steel pile wall thickness, *CCS* = (l/t) center-to-center spacing of piles in bridge longitudinal/transverse directions, respectively, in terms of number of pile diameters.

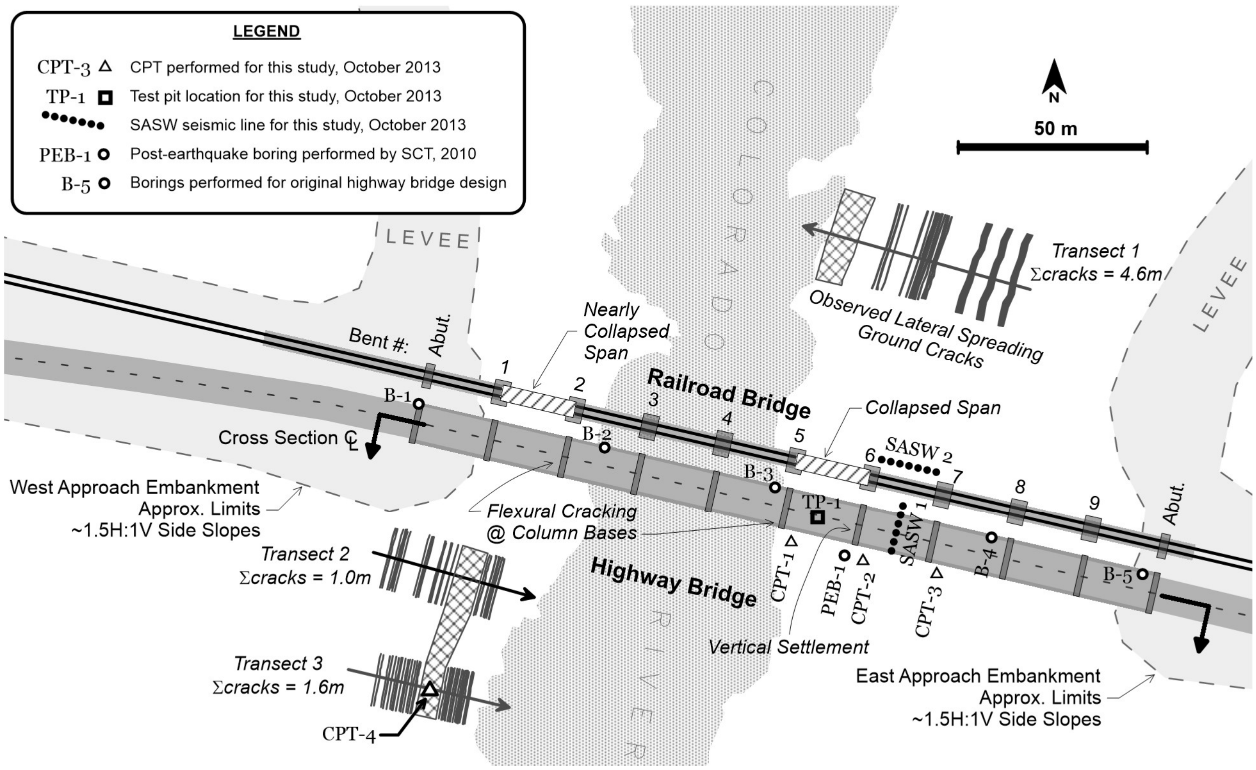

Fig. 1. Site plan showing observed damage and locations of subsurface explorations. Ground failure after GEER (2010).

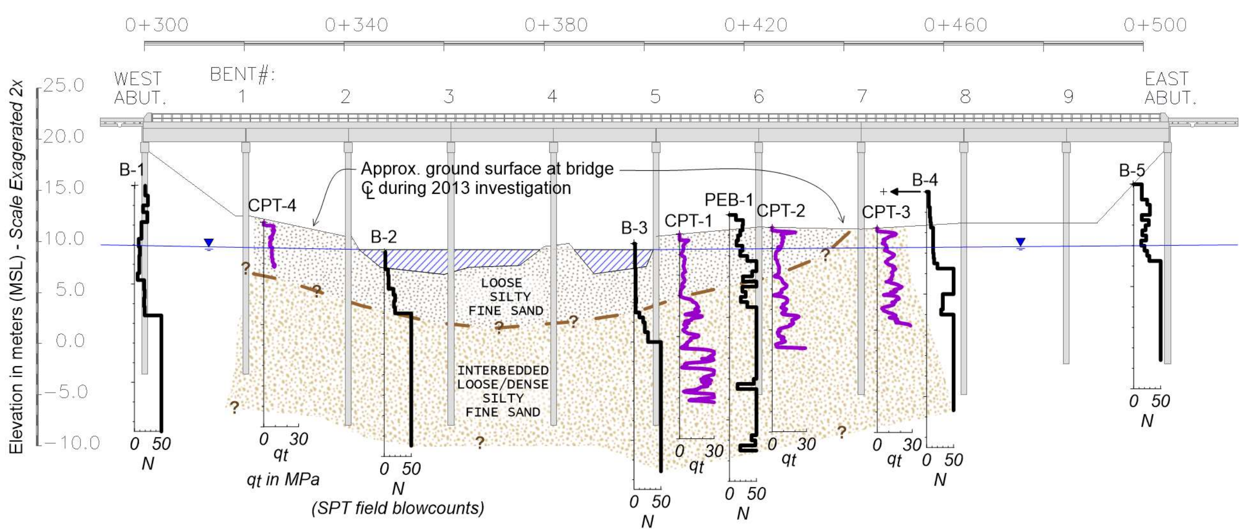

Fig. 2. Cross section along highway bridge centerline; explorations are offset from centerline as shown in Figure 1.

Fig. 3. Railroad bridge collapse due to pier translation in direction of arrow (left; photo D. Murbach) and flexural cracking of highway bridge columns in response to lateral spreading (right).

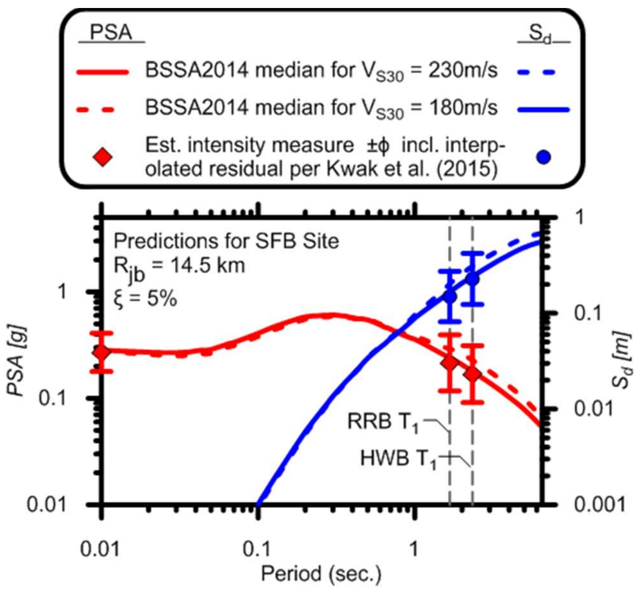

Fig. 4. Pseudo-spectral accelerations and displacements estimated for SFB site from El Mayor-Cucapah earthquake.

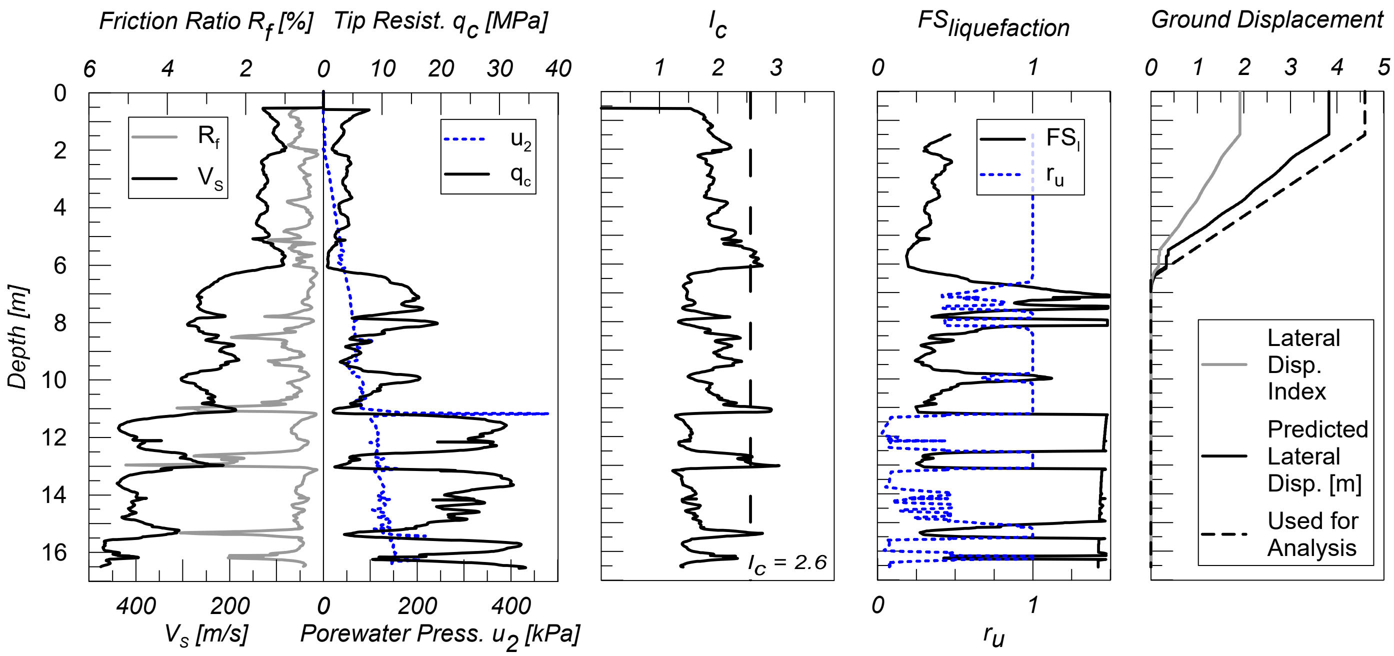

Fig. 5. Liquefaction triggering analysis for CPT-1 using PGA = 0.27 *g*. Lateral displacement estimated using Zhang et al. (2004).

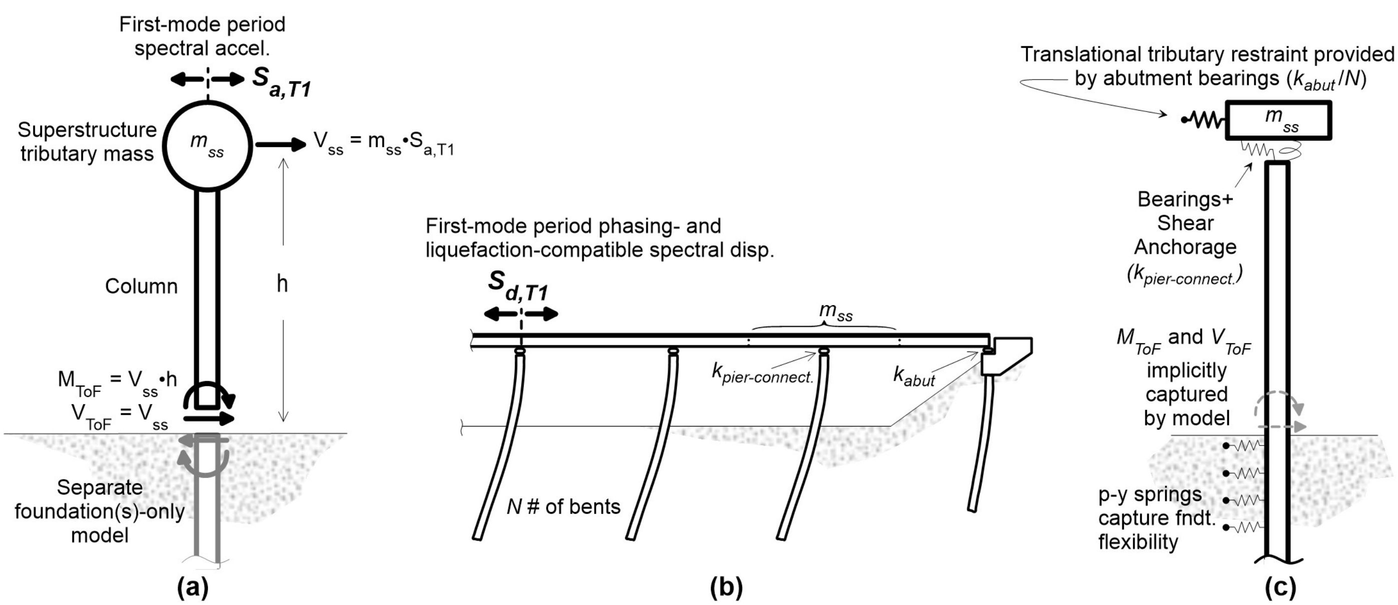

Fig. 6. (a) Caltrans (2013) force-based method for estimating top-of-foundation-level inertial shear and moment demands (V_{ToF} *and* M_{ToF}), (b) schematic of first-mode longitudinal oscillation, and (c) single-bent model for modal and lateral spreading analyses.

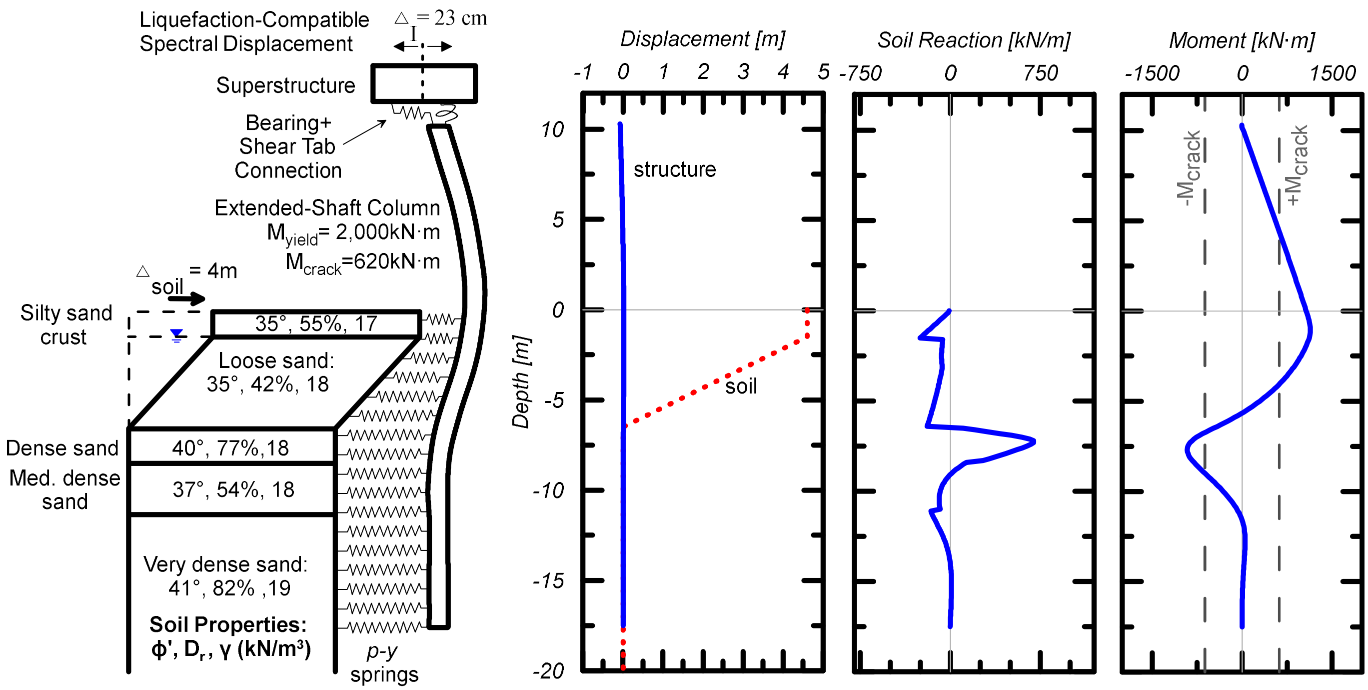

Fig. 7. Numerical models and results of Bent 5 analyses of highway (top) and railroad (bottom) bridges subjected to lateral spreading combined with inertial demands.

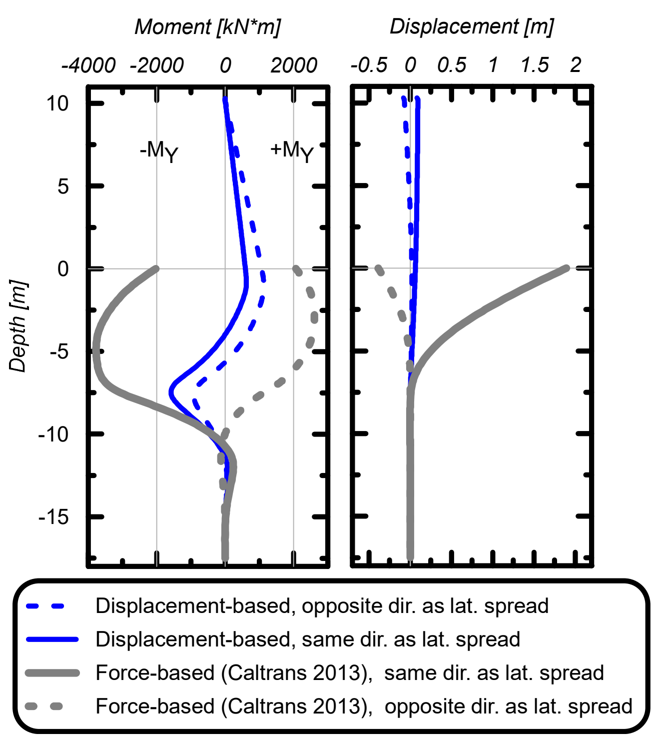

Fig. 8. Comparison of moment and displacement profiles for highway bridge piles as computed from force- and displacement-based methods for imposing superstructure inertial demands in the same and opposite directions as lateral spreading.

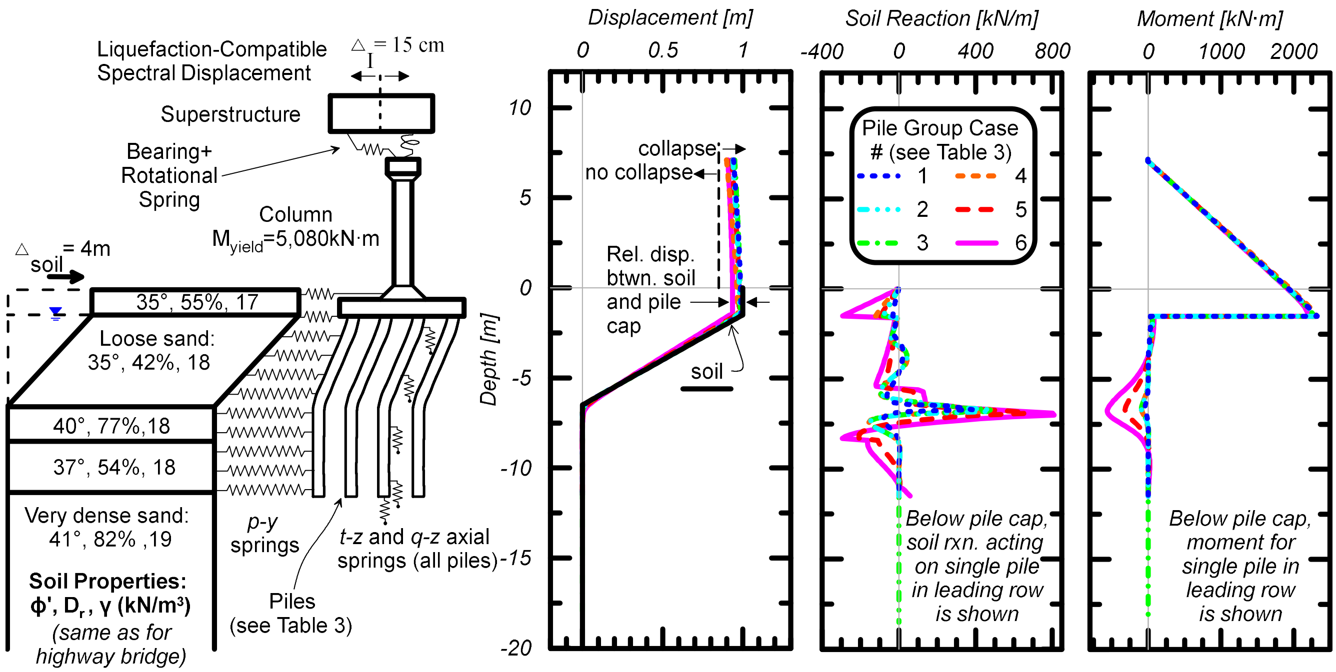

Fig. 9. Numerical model and results of Bent 5 analyses of railroad bridge subjected to lateral spreading combined with inertial demands.